

A case study using spectroscopy and computational modelling for Co speciation in a deep eutectic solvent

Isuri N. Perera,^a Garima S. Dobhal,^b Jennifer M. Pringle,^a Luke A. O'Dell,^b Sherif Abdulkader Tawfik,^b Tiffany R. Walsh,^{b*} and Cristina Pozo-Gonzalo^{a, c, d*}

^aInstitute for Frontier Materials, Deakin University, Melbourne, Victoria 3125, Australia.

^bInstitute for Frontier Materials, Deakin University, Geelong, VIC 3216, Australia.

^cAragonese Foundation for Research and Development (ARAID), Av. de Ranillas 1-D, 50018 Zaragoza, Spain.

^dInstituto de Carboquímica (ICB-CSIC), C/Miguel Luesma Castán, 4, 50018, Zaragoza, Spain.

*Corresponding author: E-mail address: cpg@deakin.edu.au; cpozo@icb.csic.es (C. Pozo-Gonzalo).

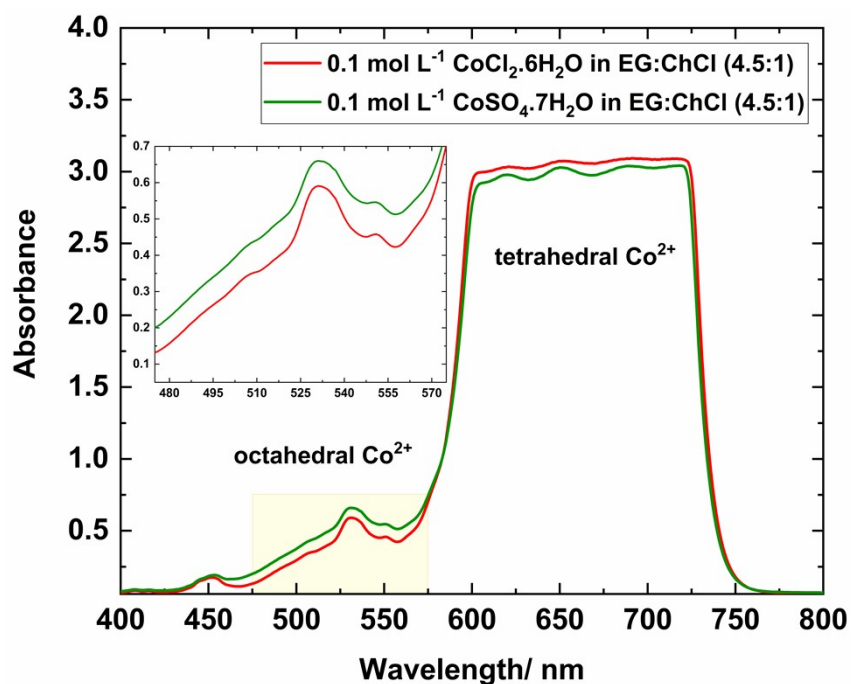


Figure S1: UV-vis spectra of 0.1 mol L⁻¹ CoCl₂·6H₂O and CoSO₄·7H₂O in EG:ChCl (4.5:1).

EPR spectroscopy

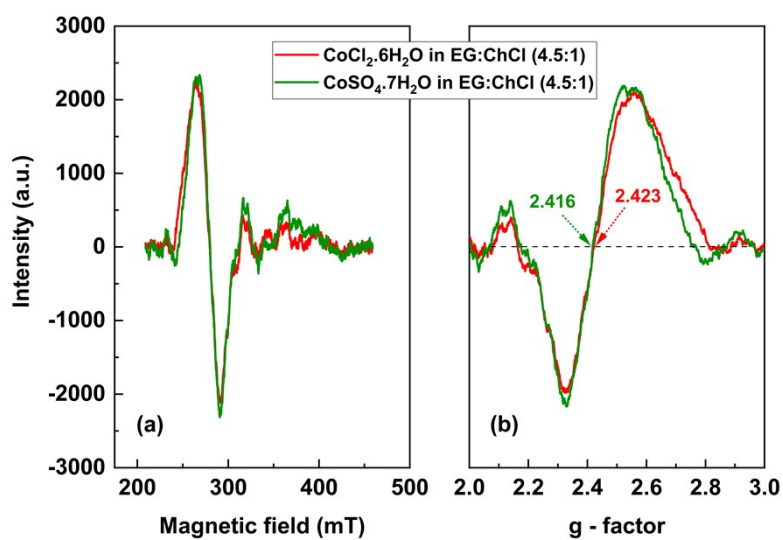


Figure S2: (a) EPR spectra and (b) calculated g-factor for 0.1 mol L⁻¹ CoCl₂·6H₂O and 0.1 mol L⁻¹ CoSO₄·7H₂O in EG:ChCl (4.5:1) at room temperature.

For a single unpaired electron ($s=1/2$) in a magnetic field, the energy splitting gap (ΔE_{Zeeman}) between ground and excited states interacting with a magnetic field is given by Equation (S1), where B_0 is the applied magnetic field strength, g_e is the free electron g value, μ_B is the Bohr magneton, ν is the frequency of the applied electromagnetic radiation (9.48 GHz in our case) and h is the plank constant.¹

$$\Delta E_{\text{zeeman}} = g_e \mu_B B_0 = h\nu \quad (\text{S1})$$

The g value is influenced by the contributions from the chemical environment and can be calculated using the below equation (S2).

$$g = h\nu / \mu_B B_0 \quad (\text{S2})$$

FTIR spectroscopy

Neat ChCl showed numerous spectral bands corresponding to O-H stretching, C-H stretching, C-H bending, C-O stretching, and C-N stretching at 3220 cm^{-1} , 3027 cm^{-1} , 1482 cm^{-1} , 1084 cm^{-1} and 953 cm^{-1} respectively, and the bands were assigned according to the literature.²⁻⁶ Neat EG showed spectral bands corresponding to O-H stretching, asymmetric C-H stretching, symmetric C-H stretching and C-O stretching at 3295 cm^{-1} , 2938 cm^{-1} , 2874 cm^{-1} , and 1083 cm^{-1} , respectively.^{2, 7} The FTIR spectrum of this specific EG:ChCl (4.5:1) shows the same profile as the spectrum reported in the literature for EG:ChCl (2:1) in terms of number of bands and band positions.^{2, 8, 7}

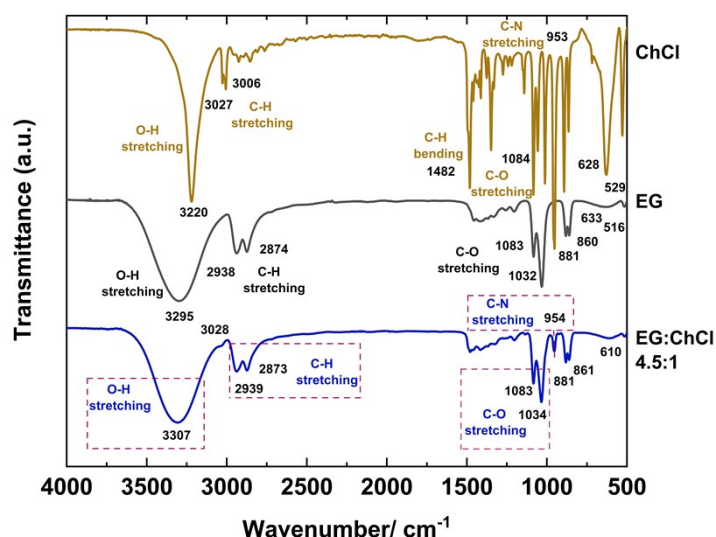


Figure S3: FTIR spectra of EG:ChCl (4.5:1) (bottom), EG (middle), and ChCl (top) analysed at room temperature.

Differences are observed between the individual compounds and the EG:ChCl (4.5:1) mixture, similar to those differences reported in the literature for other DESs.^{7,8} For instance, the broad band which corresponds to the O-H stretching (3295 cm^{-1}) in ethylene glycol has shifted to a higher wavenumber (3307 cm^{-1}) in the EG:ChCl (4.5:1). This may be due to a decrease in the extent of intermolecular OH(EG)-O(EG) bonding in the neat ethylene glycol compared to the solvent system, thus indicating interaction of ethylene glycol with the choline chloride forming H-bonds.² Wang *et al.* have reported that hydrogen bonding occurs between the chloride anion (HBA) and the H-O (HBD) ($\text{Cl} \cdots \text{H-O}$) in the DESs. This was corroborated using ^{35}Cl NMR spectroscopy, where they reported a lower chemical shift value of the chloride ion in ChCl as the DES forms.⁸ This indicates that the intensity of the newly formed H bond is weaker than the H bond formed by ChCl itself, increasing the electron density of the Cl atom and leading to an upfield shift in the chemical shift.⁸

Even though the spectrum of EG:ChCl (4.5:1) is dominated by ethylene glycol, due to its larger concentration in the mixture, features of ChCl can be observed as a shoulder at 3028 cm^{-1} and a band at 954 cm^{-1} corresponding to C-H stretching and C-N stretching respectively.²

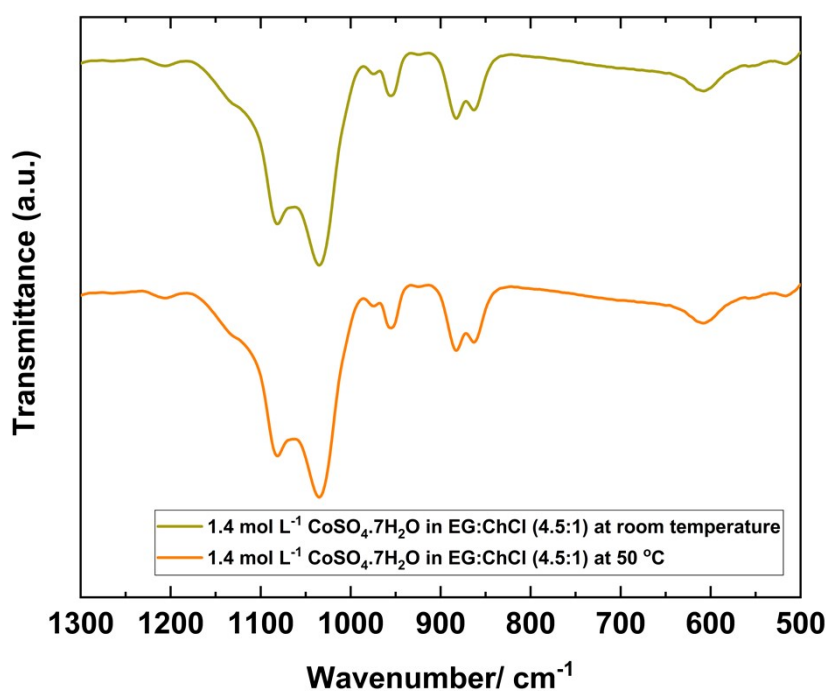


Figure S4: FTIR spectra of 1.4 mol L^{-1} of $\text{CoSO}_4 \cdot 7\text{H}_2\text{O}$ in EG:ChCl (4.5:1) analysed at room temperature (top) and $50\text{ }^\circ\text{C}$ (below).

¹H NMR Spectroscopy

EG showed two peaks corresponding to the four hydrogens of two -CH₂ groups at $\delta = 3.75$ ppm (s, 4H), labelled as “x” and two hydrogens of two hydroxyl groups at $\delta = 5.40$ ppm (s, 2H), labelled as “z” (Figure 6), whereas ChCl presented a peak for the three -CH₃ groups ($\delta = 3.21$ ppm (s, 9H)) attached to the N⁺ labelled as “d,” two hydrogens in -CH₂ attached to the N⁺ labelled as “c” ($\delta = 3.52 - 3.54$ ppm (t, 2H)), two hydrogens in -CH₂ attached to the OH labelled as “b” ($\delta = 4.05 - 4.08$ ppm (m, 2H)) and the hydrogen of the hydroxyl group labelled as “a” ($\delta = 4.75$ ppm (s, 1H)).

In the EG:ChCl (4.5:1), all peaks are shifted relative to the pure constituents, indicating changes in their average surrounding chemical environment as reported previously.⁹ The -OH group of EG is known to interact with the Cl⁻ of ChCl through H-bonding as a result of the formation of a DES.^{2, 8, 9} For instance, the -OH group (z) and aliphatic protons (x) of the EG both shifted upfield in the DES and this could be due to the interaction of the Cl⁻ of ChCl with the OH group of EG. Shifts to lower ppm values (upfield/ shielded) mean the electron density of the hydroxyl proton (z) (to a higher extent compared to aliphatic protons) and aliphatic protons (x) has increased, showing that the interaction with the ChCl could come from the -OH group. In contrast, protons of ChCl have shifted downfield in the DES, showing a decrease in the electron density of the protons. The Cl⁻ anion is a very electronegative atom, and its interaction with the -OH group of EG could be responsible for the overall change in electron density. Nuclear Overhauser Effect Spectroscopy (NOESY) spectra reported by Delso *et al.* also demonstrated this interaction between EG and ChCl in 2:1 molar ratio in the presence of water.¹⁰

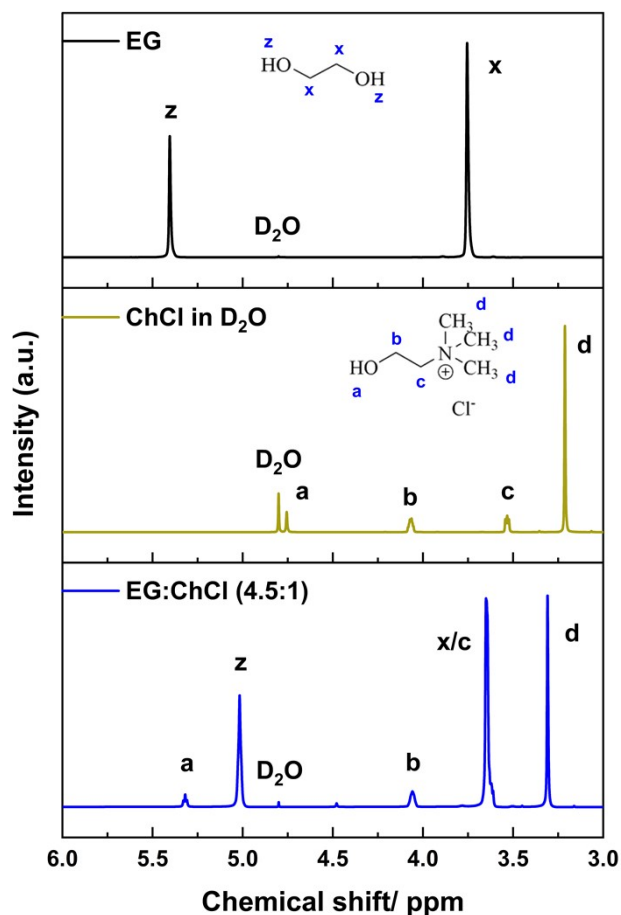


Figure S5: ^1H NMR spectra of EG (top), ChCl dissolved in D_2O (middle), and EG:ChCl (4.5:1) (bottom) analysed at room temperature.

Additionally, the chemical shift of the aliphatic protons labelled as “x” for EG and “c” for ChCl are overlapping, showing in the DES as a peak and a shoulder that is difficult to deconvolute, at approximately $\delta = 3.65$ ppm, which has also been previously observed for EG:ChCl (2:1) with 8.5 % wt water.⁹⁻¹¹ The rest of the chemical shifts could be identified at $\delta = 3.30$ ppm (s, 9H), 4.05 ppm (s, 2H) and 5.30 - 5.32 ppm (m, 1H) corresponding to “d,” “b” and “a” of ChCl as shown in Figure 6. A small peak was observed at 4.47 ppm (Figure 6) in the EG:ChCl (4.5:1) that could be related to the water in the solvent system.^{10, 11} The integration data (Figure S6) agrees with the presence of twenty hydrogens (s, 20H) in the “x+c” confirming the molar ratio formed between EG and ChCl in the solvent system.

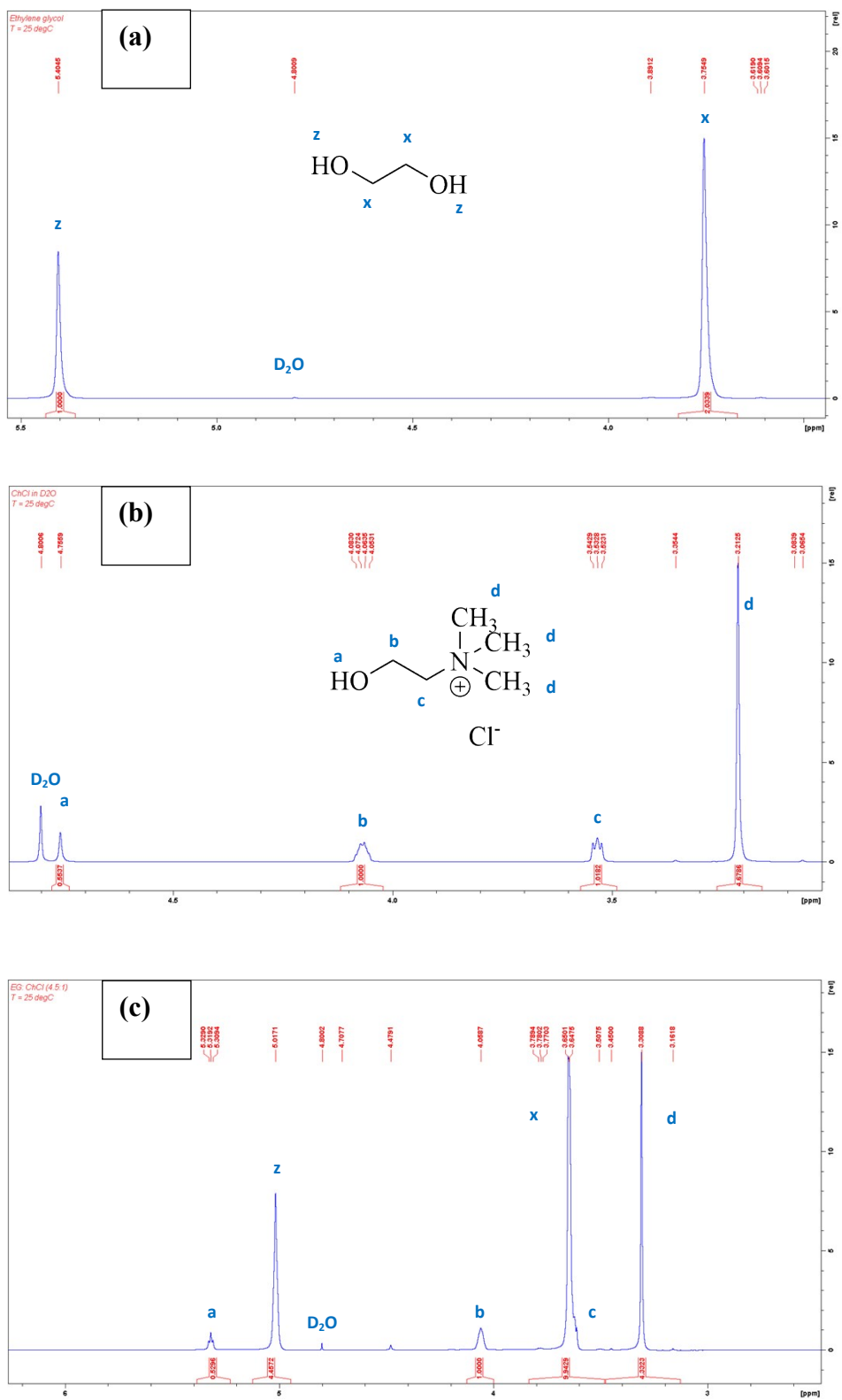


Figure S6: ^1H NMR spectra of (a) EG, (b) ChCl in D_2O and (c) EG:ChCl (4.5:1) analysed at room temperature.

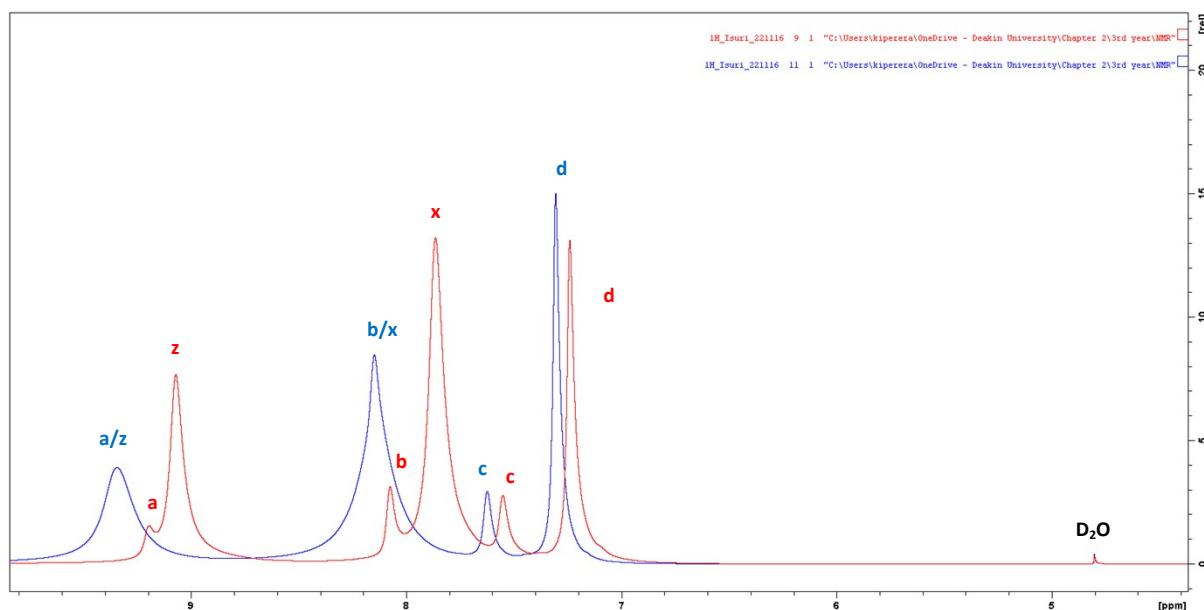


Figure S7: ¹H NMR spectra of (red) 0.1 mol L⁻¹ CoCl₂·6H₂O in EG:ChCl (4.5:1) and (blue) 0.1 mol L⁻¹ CoSO₄·7H₂O in EG:ChCl (4.5:1) analysed at room temperature.

Further details on Force Field Molecular Dynamics Simulations:

For all simulations, pressure was controlled using the Berendsen barostat with a time constant of 1.0 ps and compressibility of $4.5 \times 10^{-5} \text{ bar}^{-1}$.¹² Temperature was controlled using the Nosé-Hoover thermostat with a time constant of 0.2 ps.^{13, 14} Coloumbic and van der Waals cut-offs of 1.6 nm were used and long range electrostatics were calculated using the Particle-mesh Ewald method.^{15, 16} A timestep of 1 fs was used.

Simulated Annealing protocol:

Several simulated annealing protocols were trialed with longer quenching times, and lower top temperatures. Here, we failed to see a convergence of the radial distribution functions (RDFs) and therefore, the structuring. This was particularly when the radial distribution functions of Co- (solvent atom) were constructed which showed that the cobalt coordination environment could get easily trapped in an energy minima which could not be recovered after another cycle of heating and cooling. The SA protocol that showed the least variations in the RDFs was used for further annealing. This involved heating the system up from 300 K to 1200 K in 200 ps, keeping the temperature at 1200 K for 3 ns and cooling down to 300 K in 6 ns. After this, a 300 ps simulation under a constant number, volume and temperature ensemble (NVT) was run at 300 K during which the RDFs for cycles were recorded.

Production runs:

For our production runs, three representative states were taken from each simulated annealing cycle. Trajectories were visualised using Visual Molecular Dynamics (VMD).¹⁷ RDFs were calculated using the gmx rdf utility. Analysis of coordination numbers and H-bonding was done using in-house python codes which utilised MDAnalysis. H-bonding was calculated by using a cut-off of donor oxygen-acceptor oxygen distance of 3 Å and an angle cut-off of acceptor oxygen-donor oxygen-hydrogen of 30° or less. CN histograms for the first-shell used atom-atom cut-offs for Co-Cl, Co-O(EG), Co-NA, Co-Ow and Co-O(SO₄) using the distance at which the respective RDFs were at a minimum after the initial peak. Second-shell CN was calculated using cut-offs from the minimum after the first peak to the minimum after the second peak in the RDFs.

System	ID	Co ²⁺	SO ₄ ²⁻	Cl ⁻	Ch ⁺	EG	H ₂ O
CoCl ₂ .6H ₂ O in EG:ChCl (4.5:1)	1	32	0	384	320	1440	192
CoSO ₄ .7H ₂ O in EG:ChCl (4.5:1)	2	32	32	320	320	1440	224
CoSO ₄ .7H ₂ O in EG:ChCl (4.5:1) - Experimental concentration	6	8	8	213	213	960	56

Table S1: Samples used for classical MD simulations

AIMD system construction

Systems 1, 2, 3 and 4 are labelled according to respective concentrations of the constituents – see table S2. First, a smaller system with 1 cobalt ion, and the respective number of molecules was constructed using an unscaled force field. This system was minimised using a steepest descent algorithm. After this, the systems underwent a short 1 ns NPT equilibration until a stable density was attained. This density was in line with the experimental liquid density for the 2:1 and 4.5:1 systems. After this, the samples were annealed by heating up from 300 K to 1800 K in 200 ps and cooled down to 300 K in 1 ns to ensure the samples were well-mixed. This annealing cycle was repeated 3 times and after the radial distribution functions were consistent for two consecutive cycles. A final 200 ps NVT equilibration was done and the final frame of this was used for the ab initio MD simulations.

System	ID	Co²⁺	SO₄²⁻	Cl⁻	Ch⁺	EG	H₂O	Total atoms	Trajectory duration
CoCl ₂ .6H ₂ O in EG:ChCl (4.5:1)	1	1	0	12	10	45	6	697	20.5 ps
CoSO ₄ .7H ₂ O in EG:ChCl (4.5:1)	2	1	1	10	10	45	7	703	21.2 ps
CoSO ₄ .7H ₂ O in EG:ChCl (4.5:1) – Octahedral system 1	5	1	1	2	2	25	3	309	10.7 ps
CoSO ₄ .7H ₂ O in EG:ChCl (4.5:1) – Octahedral system 2	6	1	1	9	9	36	1	567	9.9 ps

Table S2: Samples studied for AIMD simulations

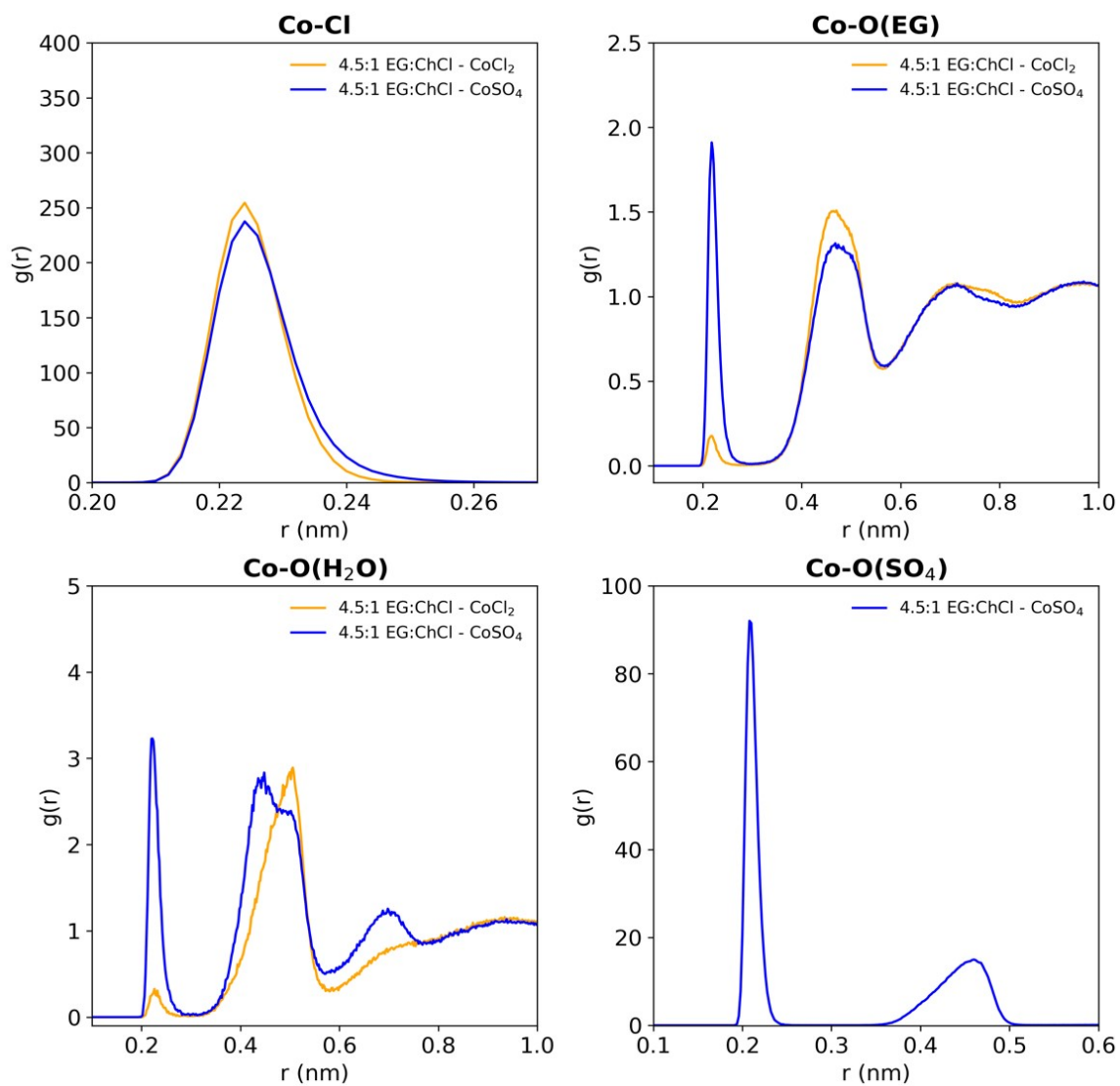


Figure S8: Radial Distribution Functions of Co-Cl, Co-O(EG), Co-O(H₂O) and Co-O(SO₄)

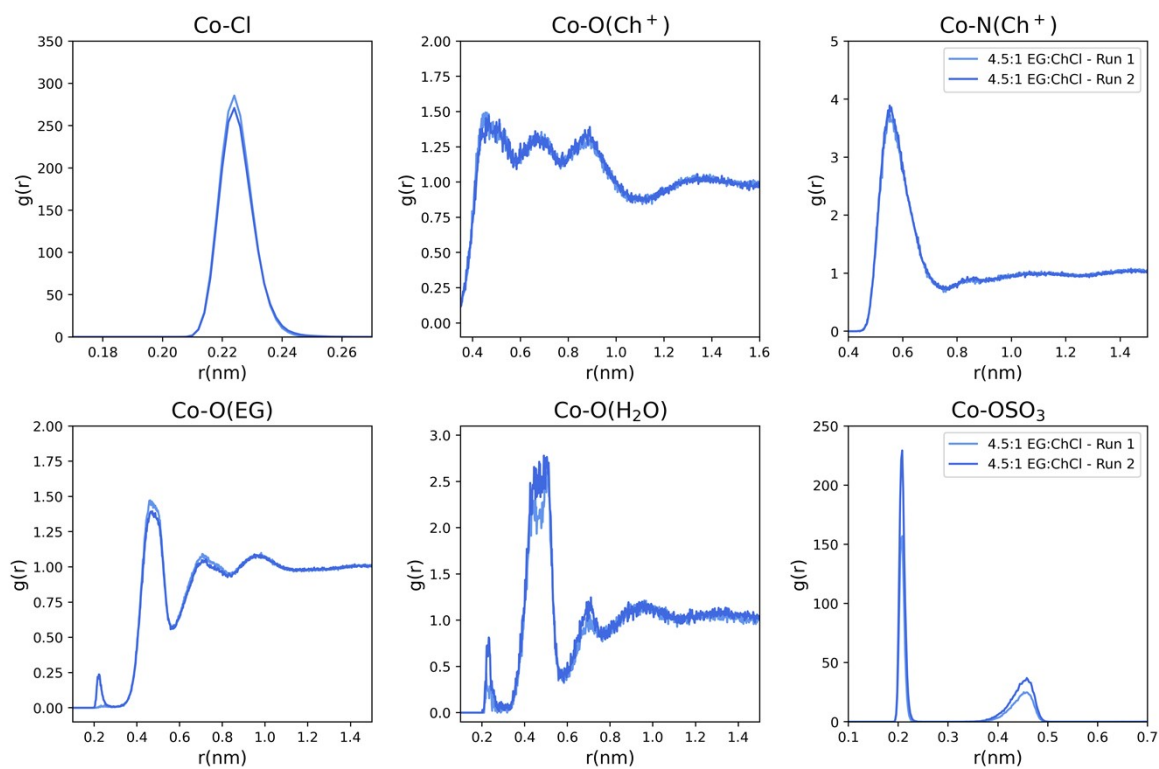


Figure S9: RDFs for experimental concentrations of CoSO_4 in the EG:ChCl (4.5:1).

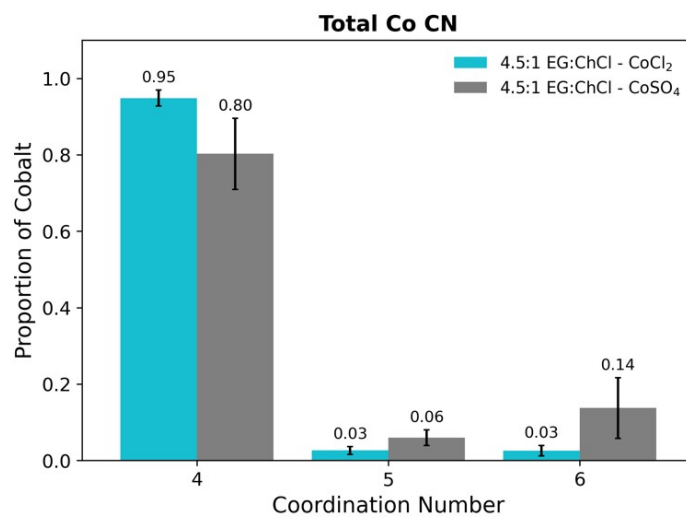


Figure S10: Total CN of Co^{2+} (CoCl_2 and CoSO_4 salts) in EG:ChCl (4.5:1).

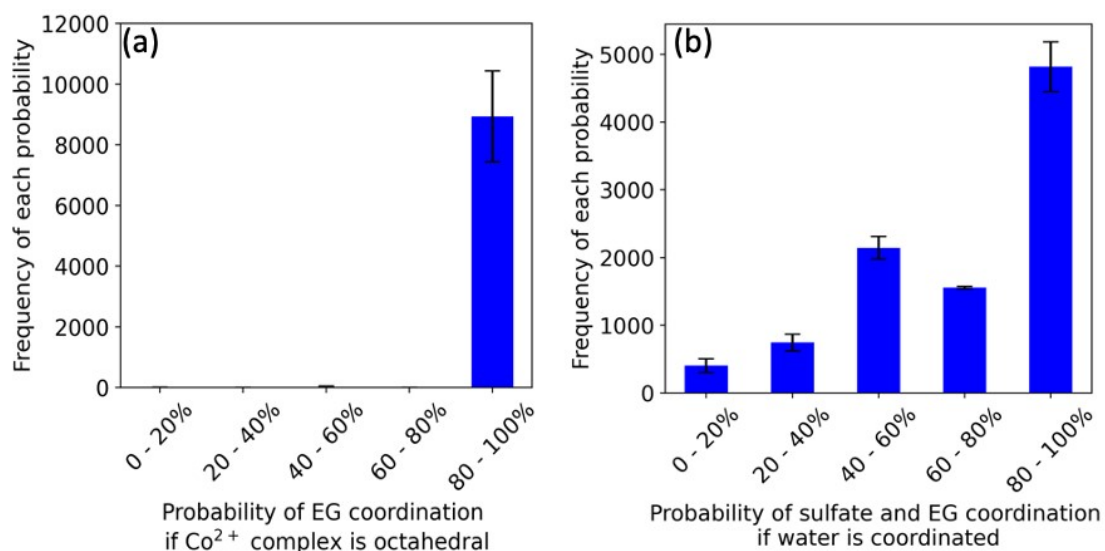


Figure S11: (a) Probabilities of EG coordination to Co^{2+} if cobalt complex is octahedral. (b) binned probabilities of sulfate and EG coordination to the cobalt if water is already coordinated to a Co^{2+} .

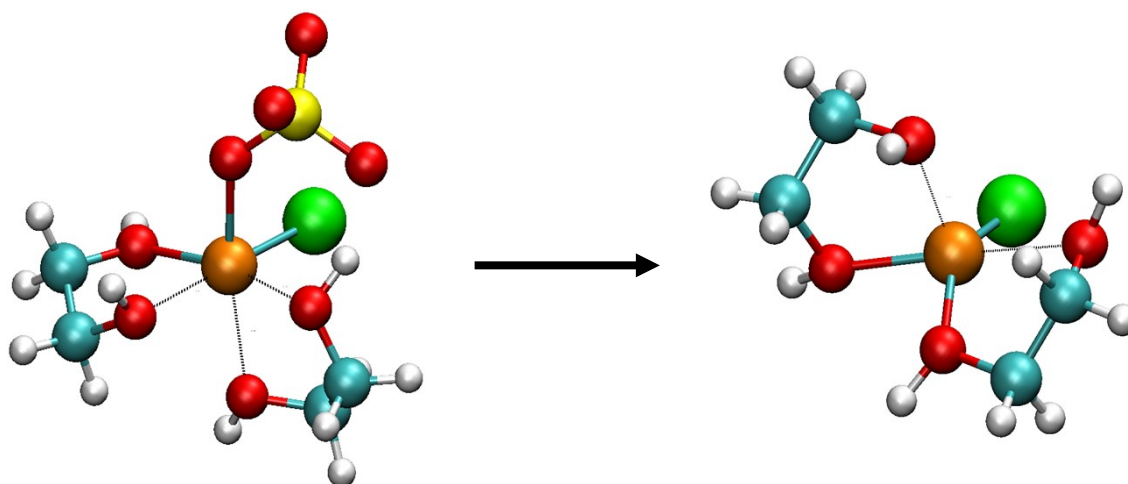


Figure S12: Initial and final state of AIMD system 6 probing octahedral coordination of Co^{2+} with no water in the first shell.

References

1. Prosser, K. E.; Walsby, C. J., Electron Paramagnetic Resonance as a Tool for Studying the Mechanisms of Paramagnetic Anticancer Metallodrugs. *European Journal of Inorganic Chemistry* **2016**, *2017* (12), 1573-1585.
2. Vieira, L.; Schennach, R.; Gollas, B., In situ PM-IRRAS of a glassy carbon electrode/deep eutectic solvent interface. *Phys Chem Chem Phys* **2015**, *17* (19), 12870-80.

3. Gera, R.; Moll, C. J.; Bhattacharjee, A.; Bakker, H. J., Water-Induced Restructuring of the Surface of a Deep Eutectic Solvent. *J Phys Chem Lett* **2022**, *13* (2), 634-641.
4. Zhuravlev, Y.; Gordienko, K.; Dyagilev, D.; Luzgarev, S.; Ivanova, S.; Prosekov, A., Structural, electronic, and vibrational properties of choline halides. *Materials Chemistry and Physics* **2020**, *246*.
5. Zhuang, J.; Li, M.; Pu, Y.; Ragauskas, A.; Yoo, C., Observation of Potential Contaminants in Processed Biomass Using Fourier Transform Infrared Spectroscopy. *Applied Sciences* **2020**, *10* (12).
6. Gautam, R.; Kumar, N.; Lynam, J. G., Theoretical and experimental study of choline chloride-carboxylic acid deep eutectic solvents and their hydrogen bonds. *Journal of Molecular Structure* **2020**, *1222*.
7. Ibrahim, R. K.; Hayyan, M.; AlSaadi, M. A.; Ibrahim, S.; Hayyan, A.; Hashim, M. A., Physical properties of ethylene glycol-based deep eutectic solvents. *Journal of Molecular Liquids* **2019**, *276*, 794-800.
8. Wang, H.; Liu, S.; Zhao, Y.; Wang, J.; Yu, Z., Insights into the Hydrogen Bond Interactions in Deep Eutectic Solvents Composed of Choline Chloride and Polyols. *ACS Sustainable Chemistry & Engineering* **2019**, *7* (8), 7760-7767.
9. D'Agostino, C.; Harris, R. C.; Abbott, A. P.; Gladden, L. F.; Mantle, M. D., Molecular motion and ion diffusion in choline chloride based deep eutectic solvents studied by ¹H pulsed field gradient NMR spectroscopy. *Phys Chem Chem Phys* **2011**, *13* (48), 21383-91.
10. Delso, I.; Lafuente, C.; Muñoz-Embid, J.; Artal, M., NMR study of choline chloride-based deep eutectic solvents. *Journal of Molecular Liquids* **2019**, *290*.
11. AlZahrani, Y. M.; Britton, M. M., Probing the influence of Zn and water on solvation and dynamics in ethaline and reline deep eutectic solvents by (¹H) nuclear magnetic resonance. *Phys Chem Chem Phys* **2021**, *23* (38), 21913-21922.
12. Berendsen, H. J. C.; Postma, J. P. M.; van Gunsteren, W. F.; DiNola, A.; Haak, J. R., Molecular dynamics with coupling to an external bath. *The Journal of Chemical Physics* **1984**, *81* (8), 3684-3690.
13. Hoover, W. G.; Holian, B. L., Kinetic moments method for the canonical ensemble distribution. *Physics Letters A* **1996**, *211* (5), 253-257.
14. Nosé, S., A unified formulation of the constant temperature molecular dynamics methods. *The Journal of Chemical Physics* **1984**, *81* (1), 511-519.
15. Darden, T.; York, D.; Pedersen, L., Particle mesh Ewald: An N·log(N) method for Ewald sums in large systems. *The Journal of Chemical Physics* **1993**, *98* (12), 10089-10092.
16. Essmann, U.; Perera, L.; Berkowitz, M. L.; Darden, T.; Lee, H.; Pedersen, L. G., A smooth particle mesh Ewald method. *The Journal of Chemical Physics* **1995**, *103* (19), 8577-8593.
17. Humphrey, W.; Dalke, A.; Schulten, K., VMD: visual molecular dynamics. *J Mol Graph* **1996**, *14* (1), 33-8, 27-8.